https://doi.org/10.5194/egusphere-2025-2844
Preprint. Discussion started: 30 June 2025

Unraveling the Impact of Heterogeneity and Morphology on Light Absorption Enhancement of Black Carbon-Containing Particles

Jing Wei[1], Jin-Mei Ding[2], Yao Song[1], Xiao-Yuan Wang[2], Xiang-Yu Pei[1], Sheng-Chen Xu[2], Fei Zhang[1], Zheng-Ning Xu[1], Xu-Dong Tian[2], Bing-Ye Xu[2], Zhi-Bin Wang[1,3]

[1] State Key Laboratory of Soil Pollution Control and Safety, Zhejiang Provincial Key Laboratory of Organic Pollution Process and Control, College of Environmental and Resource Sciences, Zhejiang University, Hangzhou 310058, China

[2] Ecological and Environmental Monitoring Center of Zhejiang Province, Hangzhou 310012, China

[3] ZJU-Hangzhou Global Scientific and Technological Innovation Center, Zhejiang University, Hangzhou 311200, China

Correspondence: Bing-Ye Xu (xubingye@zjemc.org.cn) and Zhi-Bin Wang (wangzhibin@zju.edu.cn)

https://doi.org/10.5194/egusphere-2025-2844
Preprint. Discussion started: 30 June 2025

Abstract

Black carbon (BC) is a strong climate forcer, but considerable uncertainty remains in estimating its radiative impact, largely due to persistent gaps between observed and modeled light absorption enhancement (E_{abs}). In this study, we employed a Centrifugal Particle Mass Analyzer and Single Particle Soot Photometer tandem system to characterize mass ratio (M_R, coating-to-BC) and morphology of BC-containing particles in Hangzhou, China. Fortunately, low, medium, and high E_{abs} values were observed during a single field campaign. Results show that the uniform core-shell Mie model overestimated E_{abs} especially in clean conditions (low E_{abs}). A morphology-dependent correction scheme was developed to improve optical property estimates of BC in the "transition state." This improved model better reproduces measured E_{abs} in different pollution conditions and reveals that the concentrations of particle chemical composition affect the M_R threshold defining this state. Our findings highlight the need to account for real-world particle complexity in climate-relevant BC modeling.

1 Introduce

Black carbon (BC) is a strongly light-absorbing aerosol that effectively absorbs solar radiation, warms the atmosphere, and contributes to direct radiative forcing (DRF)(Bond and Bergstrom, 2006; Seinfeld, 2008). According to IPCC assessments, the global effective DRF of BC ranges from −0.28 to 0.41 W/m^2 (Szopa et al., 2021). Most climate models(Bauer et al., 2013; Chen et al., 2024; Stier et al., 2005; Wang et al., 2023; Zhang et al., 2025) use Mie theory to estimate BC light absorption enhancement (E_{abs}), assuming a uniform core-shell structure where BC core is fully coated by coating materials. This approach predicts a monotonic increase in E_{abs} with the coating-to-core mass ratio (M_R), often reaching values up to ~2, consistent with laboratory results (Peng et al., 2016). However, field observations commonly report lower E_{abs} values, typically around 1.4 and sometimes as low as 1.09 (Cappa et al., 2012; Huang et al., 2024). This discrepancy mainly stems from the oversimplified assumptions in Mie theory, which fail to capture the real atmospheric complexity in BC size distribution, morphology, and mixing state (Wang et al., 2021c). These limitations introduce considerable uncertainty in assessing the radiative impacts of BC. Therefore, improving our understanding of the mechanisms controlling BC E_{abs} and its atmospheric evolution is essential for reducing uncertainties in BC DRF estimates and enhancing the accuracy of climate model projections.

Previous studies have explored the discrepancies in BC E_{abs} from various perspectives. A recent particle-resolved model study reveals that particle-to-particle heterogeneity in M_R significantly influences E_{abs} (Fierce et al., 2020). Traditional spherical core-shell models tend to overestimate E_{abs}, especially for partially coated particles with low M_R. However, M_R heterogeneity alone cannot explain low E_{abs} under high M_R conditions (Huang et al., 2024). Atmospheric BC particles also vary in morphology. Fresh BC exhibit a branched structure that collapses into compact shapes with reduced light absorption cross-sections during aging (Moteki and Kondo, 2007; Romshoo et al., 2024; Li et al., 2024). Early aging stage feature uneven coatings, while aged particles show BC core either encapsulated or located near the particle surface.

https://doi.org/10.5194/egusphere-2025-2844
Preprint. Discussion started: 30 June 2025

These configurations further influence E_{abs}. Recent studies suggest that the proportion of non-spherical BC particles and the position of the BC core may be key factors contributing to low E_{abs}, leading to an overestimation by core-shell model (Huang et al., 2024; Chen et al., 2024; Zhang et al., 2022). Thus, due to M_R heterogeneity and the morphological complexity, the mechanisms driving BC E_{abs} remain poorly understood, necessitating further research into relevant physical and chemical processes.

In this study, a suite of state-of-the-art instruments were employed to simultaneously capture the magnitude and dynamic evolution of M_R and morphology of BC-containing particles in Hangzhou, China. Fortunately, field measurements directly revealed the coexistence of high, medium, and low E_{abs} under high bulk-averaged M_R conditions. Further, the influences of M_R and morphology of BC-containing particles on E_{abs} are quantified to reconcile the discrepancies between models and observations under different E_{abs} conditions. Subsequently, an improved model for "transition-state" BC-containing particles was developed to reproduce the observed E_{abs} under varying E_{abs} and bulk-averaged M_R conditions. This study underscores the importance of simultaneously considering M_R heterogeneity and morphology of BC-containing particles in predicting E_{abs}. These findings contribute to reducing the uncertainty in estimating the DRF of BC.

2 Methods

2.1 Overview of the field campaign and instrumentation

The field measurements were conducted at the Central Air Quality Assurance Monitoring Station (30.25°N,120.24°E) in Hangzhou from 3th Sept., 2023 to 13th Oct., 2023. The sampling site is located just 100 meters from the Qiantang River in the western part of Hangzhou, with major traffic routes within 3 kilometers to the northeast and southwest of the station. The schematic of the instrumentation is provided in Fig. S1. Aerosols were sampled after passing through a $PM_{2.5}$ impactor and then dried through a diffusion dryer before reaching subsequent instruments. The mass of an BC-containing particle (M_p) and of the BC core (M_{BC}) can be simultaneously obtained by a Centrifugal Particle Mass Analyzer (CPMA, Cambustion) and a single-particle soot photometer (SP2, DMT Inc.) tandem system. In the CPMA-SP2 system, particles with known mass (M_p) selected by CPMA were injected into the SP2, and the M_p was set from 0.9 fg to 30 fg with a logarithmic evenly spaced distribution, divided into 10 M_p, specially 0.93 fg, 1.37 fg, 2.02 fg, 2.97 fg, 4.36 fg, 6.40 fg, 9.39 fg, 13.78 fg, 20.22 fg and 29.68 fg, then the mass of BC core was measure by SP2. The duration of one set point cycle was 1 hour, with each M_p point sampling for 5 minutes, and all M_p points was sampling for total of 50 minutes. The remaining 10 minutes were divided into 4 minutes for instrument stabilization and 6 minutes for measuring all BC-containing particles when the valve was switched to the single SP2 line. During further data analysis, particles with M_p = 0.93 fg and M_p = 1.37 fg exhibited excessively noisy scattering signals and were therefore excluded from subsequent statistical analysis. The SP2 was calibrated with size-resolved Aquadag aerosols to establish the correlation

https://doi.org/10.5194/egusphere-2025-2844
Preprint. Discussion started: 30 June 2025

between incandescence peak height and the mass of BC-containing particles (DMT, 2011) (Fig. S2c and d). As reported in previous studies (Liu et al., 2020; Liu et al., 2014; Zhang et al., 2018), a correction factor of 0.75 was applied to the peak height during calibration. The SP2 scattering signal was calibrated with polystyrene latex spheres (PSL) of known sizes (210 nm, 270 nm and 310 nm) (Fig. S2b). Additionally, the calibration of the scattering and the incandescence channels was performed before and after the measurement campaign. The mass concentrations of non-refractive OA, nitrate, sulfate, ammonium and chloride was measured by an aerosol chemical speciation monitor (ACSM, Aerodyne Research Inc.).

The aerosol extinction coefficient and scattering (Fig. S3) at wavelength of 440 nm, 530 nm and 630 nm was measured by Multi-Wavelength Cavity Attenuated Phase Shift Single-Scattering Albedo Monitor (CAPS-ALB) (Weber et al., 2022), the aerosol absorption coefficient was the difference between extinction coefficient and scattering coefficient. Meanwhile, the aerosol scattering coefficient at wavelength of 450 nm, 525 nm, and 635 nm was also measured by Nephelometer (Multi Wavelength Integrating Nephelometer) (Schloesser, 2016). The slope of the scattering coefficient measured by CAPS and Nephelometer at corresponding wavelength was close to 1 (Fig. S4), indicating the all data are reliable for further analysis. Besides, before sampling, the scattering coefficient of CAPS and Nephelometer at every wavelength was calibrated using PSL spheres. The slope of the scattering coefficient measured by CAPS (or the Nephelometer) and modeled by Mie theory was close to 1 (Fig. S5), indicating the reliability of the CAPS and Nephelometer. The lower detection limit of the Nephelometer at all three wavelengths was 0.3 Mm^{-1} with a 60-second integration time, while that of the CAPS was 1 Mm^{-1} with 30-second integration time.

2.2 Mixing state and morphology of the particle-resolved BC-containing particles

The mixing state of single BC-containing particle can be represented by the mass ratio of the BC coating to BC core without any assumptions,

$$M_R = \left(M_p - M_{BC}\right)/M_{BC} \quad (1)$$

where M_p and M_{BC} were the mass and core of each BC-containing particle. Then M_R was converted to the bulk-averaged M_R to compared the measured E_{abs} in bulk particles by summing of total coating and core mass of BC-containing particles every hour,

$$bulk\ average\ M_R = \frac{\sum_i M_{R,i} \times M_{BC,i}}{\sum_i M_{BC,i}} \quad (2)$$

where i was the i^{th} single BC-containing particle. The data measured by CPMA-SP2 were corrected via several steps, including (1) correction of delay time, (2) multi-charged particles and (3) collection efficiency (for details, see Text S1).

In CPMA-SP2, when knowing M_p and M_{BC}, the modeled scattering cross section ($C_{modeled}$) of BC-containing particles can be derived using Mie theory (Wang et al., 2021a). This calculation assumes a core-shell structure with BC having refractive index of 2.26–1.26i (Liu et al., 2017; Zhao et al., 2020) and the coating with 1.48i, along with a coating density of 1.5 g cm^{-3} (Liu et al., 2015). The measured scattering cross section ($C_{measured}$) is analyzed using the leading-edge-only (LEO) technique, which reconstructs

https://doi.org/10.5194/egusphere-2025-2844
Preprint. Discussion started: 30 June 2025

the distorted scattering signal when BC-containing particles passes through the SP2 laser beam, as widely described in previous studies (Liu et al., 2014; Zhang et al., 2016; Brooks et al., 2019; Gao et al., 2007; Zhang et al., 2020). Note only particles with successfully fitted LEO signals are considered in the optical property calculations. Subsequently, $C_{modeled}$ can be compared with $C_{measured}$ to infer the morphological characteristic of BC-containing particles (Liu et al., 2017; Liu et al., 2020). Further details can be seen in Section 3.

2.3 The measured and modeled E_{abs}

The light absorption enhancement of BC-containing particles is defined as the ratio of the mass absorption cross section (MAC) of the coated and uncoated BC-containing particles,

$$E_{abs\_measured} = \frac{MAC_{BC}}{MAC_{BC\_core}} \quad (3)$$

where $E_{abs\_measured}$ is the measured light absorption enhancement, and MAC_{BC_core} is the mass absorption coefficient for uncoated BC particles. The value of MAC_{BC_core} was obtained by extrapolating MAC_{BC} to the limit of bulk-averaged $M_R = 0$. The MAC_{BC_core} at wavelength of 630 nm was 9.08 (Fig. S6).

The commonly used models for calculating the optical properties of BC-containing particles include Core-shell Mie theory (Cappa et al., 2012), T-matrix (Wu et al., 2020), and discrete dipole approximation (DDA) (Kahnert and Kanngießer, 2020). Among them, T-matrix, and DDA fully account for the impact of morphology of BC-containing particles by incorporating detailed three-dimensional parameters such as fractal dimension and monomer number (Wu et al., 2020). In contrast, Core-shell Mie theory relies solely on the BC core size (D_c) and coating thickness (D_p/D_c). Given the measurement data available in this study, the Core-shell Mie theory was used to calculate the E_{abs} of BC-containing particles in this study. The refractive index (RI) of BC and its coatings are assumed to be n=1.85+0.71i and n=1.5+0i (Liu et al., 2015; Liu et al., 2014). The size of BC core and coating thickness was directly measured by CPMA-SP2 tandem system. For the uniform core-shell assumption, the M_R of every D_c was equal to bulk-averaged M_R (Method), as described by Cappa et al. (2019) and Liu et al. (2017). Then the particle-resolved Core-shell Mie theory was employed to calculate the MAC_{BC} of individual BC-containing particles. After obtaining the particle-resolved MAC, we can calculate the MAC of BC particle ensembles as

$$MAC_{BC} = \sum_{i=0}^{n} MAC_i \times \frac{[BC]_i}{[BC]} \quad (4)$$

where MAC_i and $[BC]_i$ are the particle-resolved MAC_{BC} and mass concentration of the BC core, [BC] is the mass concentration of BC particle ensembles, and n is the number of M_p bins. Then, the E_{abs} of BC particle ensembles are calculated as the ratio of MAC_{BC} to MAC_{BC_core}. Note that the MAC_{BC_core} here is calculated using the core-shell Mie model when $D_p / D_c = 1$.

The morphology-dependent approach was based on the $C_{measured}$ measured by SP2 and $C_{modeled}$ by Core-shell Mie theory at wavelength of 1064 nm. The approach mainly primarily focuses on calculating the optical properties of transition-state BC-containing

https://doi.org/10.5194/egusphere-2025-2844
Preprint. Discussion started: 30 June 2025

particles based on their morphology. In this study, we use the scattering cross-section of transition-state BC-containing particles measured by SP2 at 1064 nm as a reference, establish a mathematical relationship between the $C_{measured}$ and M_R (Fig. 3d, e and f), and use this relationship to calculate the MAC of this portion of BC-containing particles. Then the bulk-averaged MAC was obtained by integrating the MAC of each BC-containing particle.

3 Results and discussions

3.1 Direct observation of different E_{abs}.

The average $E_{abs\_measured}$ during the sampling period in Hangzhou is 1.28, and the bulk-averaged M_R is 3.32. Based on the measured E_{abs}, three scenarios were identified (Fig. S7 and Fig. 1). Case 1 spans from September 3 to September 23, 2023, and from October 1 to October 7, 2023. Case 2 covers the period from September 24 to September 30, 2023, while Case 3 runs from October 8 to October 13, 2023. $E_{abs\_measured}$ in Case 1 is relatively low, with an average value of 1.09. In contrast, the $E_{abs\_measured}$ in Case 2 and Case 3 is significantly higher, with average values of 1.84 and 1.55, respectively.

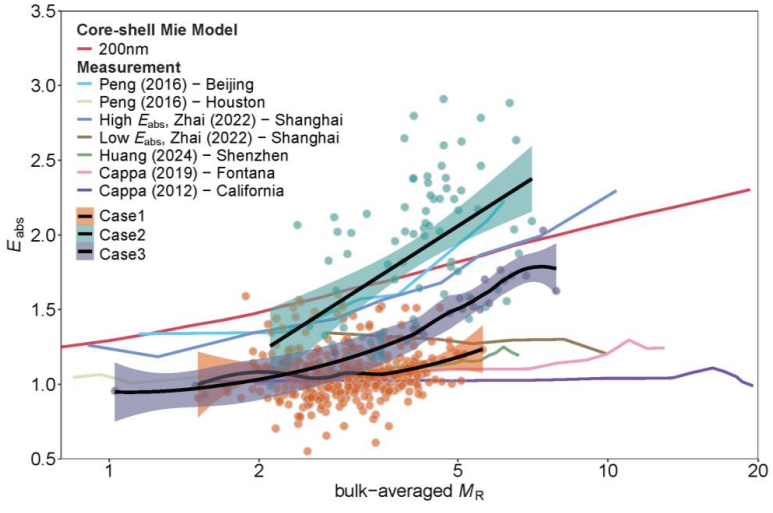

Figure. 1 Comparison of measured E_{abs} in different observation periods and with previous studies (Peng et al., 2016; Cappa et al., 2012; Zhai et al., 2022; Cappa et al., 2019; Huang et al., 2024). The black solid line represents the fitted smoothing curve of bulk-averaged M_R and measured E_{abs}, with the shaded area indicating the 95% confidence interval of the fit.

Some studies conducted in cities such as Beijing (Peng et al., 2016), Shanghai (Zhai et al., 2022) have observed a notable increase in $E_{abs\_measured}$. However, in cleaner regions like Shenzhen (Huang et al., 2024), Houston (Peng et al., 2016) and California

https://doi.org/10.5194/egusphere-2025-2844
Preprint. Discussion started: 30 June 2025

(Cappa et al., 2012; Cappa et al., 2019), even when R_{BC} reached approximately 5, many studies reported minimal increases in $E_{abs\_measured}$. Fortunately, our observations captured a wide range of $E_{abs\_measured}$ values (0.92~1.84), encompassing high, medium, and low levels. In these three cases, $E_{abs\_measured}$ showed markedly different evolution patterns during the aging of BC-containing particle populations (Fig. 1). Specially, in Case 1, $E_{abs\_measured}$ remained almost unchanged with increasing bulk-averaged M_R. In Case 3, $E_{abs\_measured}$ showed a significant increase as bulk-averaged M_R rose, while in Case 2, the increase in $E_{abs\_measured}$ was even more pronounced for the same increment in bulk-averaged M_R. Besides, in Case 2, the E_{abs} calculated by the traditional core-shell Mie model ($E_{abs\_uniform}$) closely matches the $E_{abs\_measured}$, followed by Case 3, which shows a slightly lower level of consistency. However, in Case 1, the $E_{abs\_uniform}$ predicted by the traditional core-shell Mie model is significantly higher than the $E_{abs\_measured}$. In our subsequent analysis, we will address this discrepancy by exploring both heterogeneity of M_R and morphology.

3.2 Role of mixing state heterogeneity in E_{abs} and direct evidence of morphology of BC-containing particles with increasing coating thickness.

The measurement data were integrated and corrected to quantify the coating-to-black carbon mass ratio (M_R) and morphology of each black carbon-containing particle. The M_R is an important indicator reflecting the aging of BC (Zeng et al., 2024; Li et al., 2024; Liu et al., 2017). Fig. 2a and 2b illustrated significant differences in the normalized number distribution of BC-containing particles at M_p = 4.35 fg and 9.38 fg at different period. Specifically, during Case 2 and Case 3, the M_R presents a unimodal distribution, with the peak value increasing with increasing M_p. In contrast, during Case 1, the M_R exhibits a distinct bimodal distribution, and both peak positions shift toward higher M_R values as M_p increases. For example, when M_p = 4.35 fg, the two peaks occur at M_R = 1 fg and 4.2 fg, respectively, whereas at M_p = 9.38 fg, they shift to M_R = 1.8 fg and 8.0 fg, respectively. The standard deviation (*SD*) of $\log_{10}(M_R)$ was used to characterize the heterogeneity of M_R among individual BC-containing at each M_p. The results showed that the *SD* of Case 1 (0.63) was greater than that of Case 3 (*SD* = 0.52), followed by Case 2 (*SD* = 0.48). In contrast, the $E_{abs\_measured}$ exhibited an opposite trend during three corresponding periods, indicating that the greater M_R heterogeneity of BC-containing particles leads to a lower $E_{abs\_measured}$. This is further supported by the positive correlation between the difference in E_{abs} (modeled by the uniform core-shell Mie model and measured) and *SD* (Fig. 2d). In other words, the uniform core-shell model predicts a greater E_{abs} as M_R heterogeneity increases, which leads to a greater discrepancy between the measured and modeled E_{abs}. This discrepancy is primarily due to stems from the uniform core-shell model's simplified treatment of M_R heterogeneity in BC (Romshoo et al., 2024; Wang et al., 2021c).

https://doi.org/10.5194/egusphere-2025-2844
Preprint. Discussion started: 30 June 2025

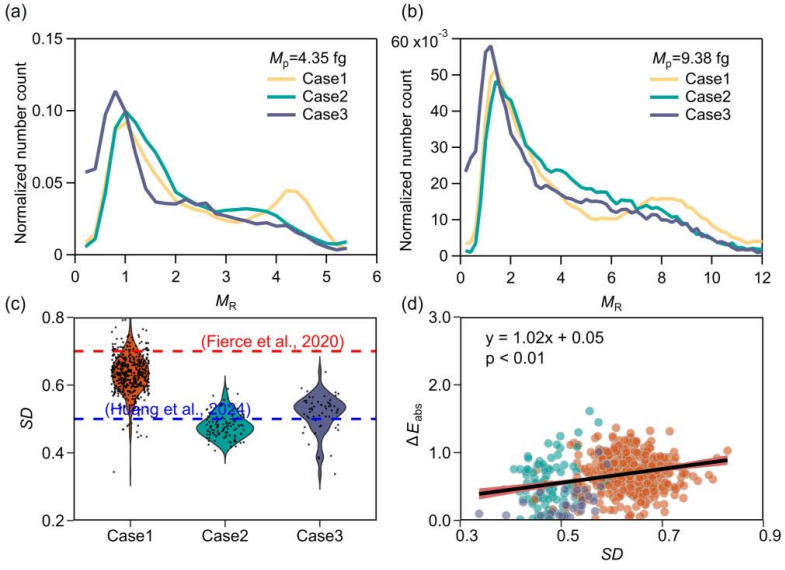

Figure. 2 Heterogeneity of BC-containing particles in different observation periods. The average M_R normalized number distribution of BC-containing particles at M_p = 4.35 fg (**a**) and M_p = 9.38 fg (**b**) during different cases. (**c**) Comparison of the average standard deviation (*SD*) of $\log_{10}(M_R)$ in this study with those reported by Huang et al. (2024) and Fierce et al. (2020), the *SD* characterizes the dispersion of M_R among individual BC-containing particles. (**d**) Linear fitting of ΔE_{abs} ($E_{abs\_uniform}$-$E_{abs\_measured}$) with the *SD* of $\log_{10}(M_R)$.

The SP2 can measure the scattering cross-section (C_{sca}) of single BC-containing particles, providing insights into their morphology. Fig. 3 presents the variation of the ratio $C_{sca\_measured}/C_{sca\_modeled}$ with M_R under different M_p. When M_R is relatively low, $C_{sca\_measured}/C_{sca\_modeled}$ is less than 1, suggesting that the BC core may exist in a fractal structure, remain bare, or are not fully embedded in the coating materials. Consequently, the measured C_{sca} is lower than that calculated by the core-shell Mie model. This observation aligns with the finding by Liu et al. (2017), who classified such BC-containing particles as externally mixed. As M_R increases, the ratio of $C_{sca\_measured}/C_{sca\_modeled}$ also increases, indicating the BC core becomes more compact and more thoroughly coated, transitioning toward a core-shell structure. Previous studies (Liu et al., 2017; Liu et al., 2020) have referred to BC in this aging stage as being in the "transition state". However, the M_R criteria for the "transition state" vary across different periods: 1.43-3.78 in Case 2, 1.45-4.19 in Case 3, and higher range of 1.78-6.34 in Case1. This implies that under polluted conditions (Case 2 and Case 3), BC particles can form core-shell structure with less coating material. This can be attributed, on the one hand, to unfavorable meteorological conditions—particularly low wind speed (0.81 m/s)—which facilitated the accumulation and formation of secondary inorganics and organics, accelerating the heterogeneous aging of BC-containing particles. On the other hand, the presence of abundant pollutants originating from

https://doi.org/10.5194/egusphere-2025-2844
Preprint. Discussion started: 30 June 2025

Jiangsu and northern Zhejiang (Fig. S7 and Fig. S8) further contributed to this rapid aging process. These factors explain why BC required less coating material to evolve into a core-shell structure in Case 2 and Case 3 compared to Case 1. When M_R exceeds the range associated with the transition state, BC-containing particles predominantly adopt a spherical shape, as further confirmed by the steady ratio of $C_{sca\_measured}/C_{sca\_modeled}$.

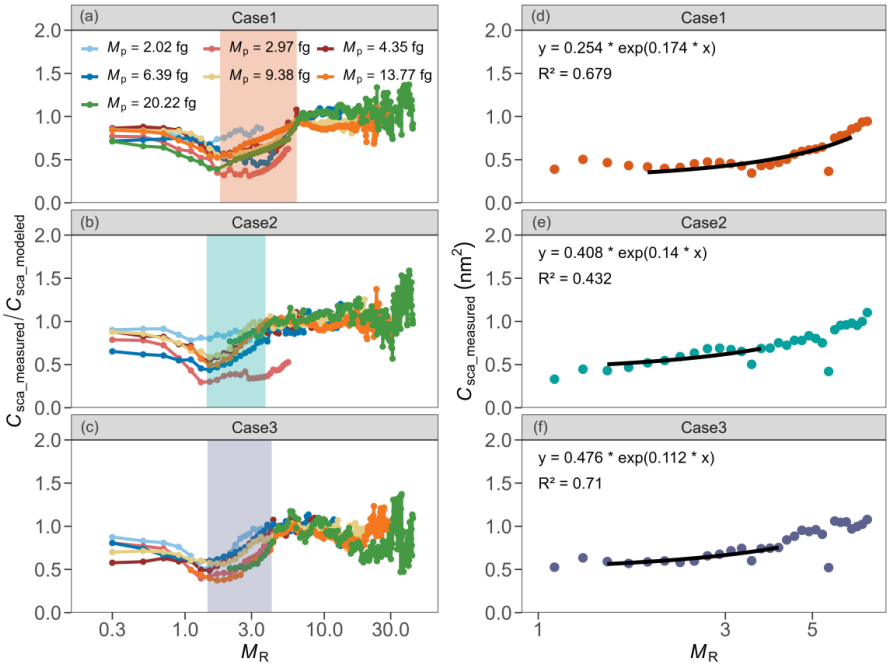

Figure. 3 The morphology and measured optical properties of BC-containing particles as a function of mass ratio (M_R). (**a**) – (**c**) show the ratio of measured to modeled scattering cross-section during different cases. The shadows indicate the M_R ranges corresponding to "transition-state" BC-containing particles. (**d**) – (**f**) present the measured scattering cross-section as a function of M_R, along with fitted morphology-dependent models representing the "transition-state" BC-containing particles.

3.3 The predicted E_{abs} during different period.

The complexity of BC in the atmosphere depends on various factors, including the size, morphology of the BC core, coating amount, and the interaction between the BC core and the coating. this study retrieves comprehensive multidimensional information on single BC-containing particle, which is subsequently incorporated into the optical model, as shown in Fig. 4. The bias between $E_{abs\_uniform}$ and $E_{abs\_measured}$ varies across different periods, even when applying the same model input scheme. Specially, the $E_{abs\_uniform}$ closely aligns with $E_{abs\_measured}$ during Case 2 and Case 3, with deviations below 10%, whereas the deviation increases to as much as to 65% during Case 1, primarily due to the higher M_R dispersion of BC-containing particles in this period. To further investigate this discrepancy, we assume that all BC-containing particles adopt a

https://doi.org/10.5194/egusphere-2025-2844
Preprint. Discussion started: 30 June 2025

core-shell morphology and calculate the E_{abs} of each BC-containing particle based on the measured single-particle M_R. Subsequently, the E_{abs} of bulk BC-containing particles was determined (Method) and compared with $E_{abs\_measured}$ to evaluate their consistency. The results show that for the Case 1, although the discrepancy between the measured and modeled values exhibits a decreasing trend, the average deviation remains as high as 38%. This finding is inconsistent with previous studies (Fierce et al., 2020), which suggest that the M_R heterogeneity of BC-containing particles can largely explain the overestimation of $E_{abs\_measured}$ by the uniform core-shell model. The discrepancy arises because the M_R dispersion of BC-containing particles in that study was lower than the observed value (Fig. 2c) in the present study. However, for Case 2 and Case 3 with higher M_R heterogeneity of BC-containing particles, the error between the model and measured E_{abs} is almost negligible, with deviations below 10%, indicating that the core-shell Mie model can reproduce the observed E_{abs} during these periods. These findings further validate that the degree of M_R dispersion of BC-containing particles is a key factor in determining whether the core-shell Mie model overestimates the observed E_{abs}, and to what extent this overestimation occurs.

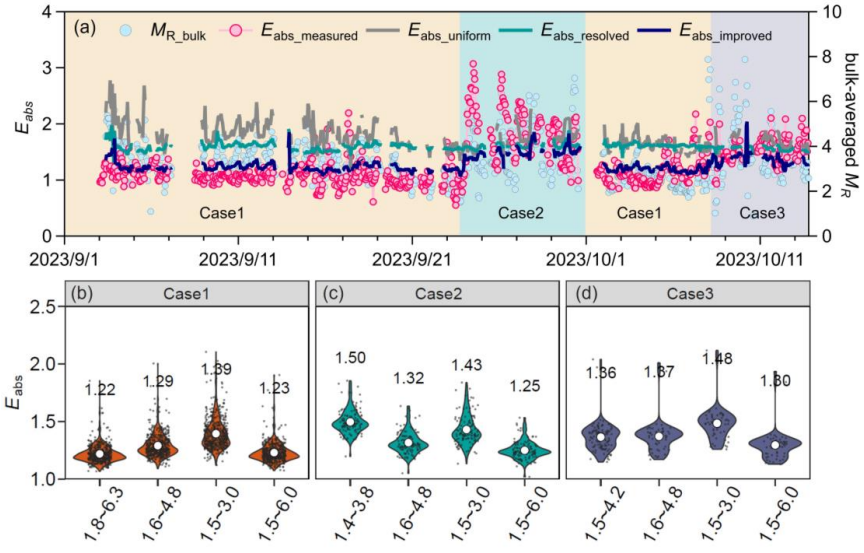

Figure. 4 Comparison of measured and modeled E_{abs} under various different model input schemes. (**a**) shows the time series of the E_{abs} during the observation period. (**b**) – (**d**) were the sensitivity of E_{abs} to the "transition state" range of BC-containing particles. The "transition state" range of 1.6~4.8 was the average value derived from Case 1, Case 2 and Case 3. The range of 1.5~3.0 and 1.5~6.0 was reported by Liu et al. (2017), and Liu et al. (2020), respectively.

The proportion of BC cores embedded in their coatings varies significantly due to differences in atmospheric conditions, which further leads to differences in E_{abs}. Under low non-volatile PM_1 and low relative humidity (RH) conditions, the proportion of BC cores embedded in the coating was small, resulting in lower E_{abs} (Cappa et al., 2019). However, during the haze period in Beijing (Zeng et al., 2024), intense liquid-phase

https://doi.org/10.5194/egusphere-2025-2844
Preprint. Discussion started: 30 June 2025

chemical reactions produced a large number of inorganic substances, causing rapid aging of BC-containing particles, which significantly increased the degree of BC core embedding and led to higher E_{abs}. The essence of this differences lies in the fact that the BC core lacks sufficient coating material to form a core-shell structure. Therefore, the embedding pattern mainly occurs in the BC-containing particles with small M_R. The chemical composition of PM_1 especially for nitrate during Case 2 and Case 3 was significantly higher than in Case 1 (Fig. S7), resulting in higher bulk-averaged M_R and E_{abs} for BC. However, during Case 1, the lower concentrations of chemical components of PM_1 was unfavorable for the formation of BC coatings, thereby leading to lower bulk-averaged M_R and E_{abs}. Therefore, a larger proportion of BC-containing particles remain in a "transition" and externally mixed state (Fig. S9), for which the E_{abs} is considered negligible. Consequently, accurately quantifying the E_{abs} of "transition state" is essential for determine the bulk E_{abs}. To address this, a morphology-dependent approach was developed to calculate E_{abs} of BC-containing particles in the "transition state", which was achieved by fitting the measured C_{sca} against M_R (Fig. 3d-3f). The improved model yielded an average E_{abs} of only 1.21 during Case 1. For Case 2 and Case 3, although the modeled E_{abs} ($E_{abs\_improved}$) were slightly lower than $E_{abs\_measured}$, the deviation remained within 20%. These findings suggest that the improved model effectively reconcile the E_{abs} of BC-containing particles under different atmospheric conditions.

In recent years, the application of particle-resolved models in multiple field observations has effectively improved the overestimation of observed E_{abs} by uniform core-shell Mie model (Fierce et al., 2020; Li et al., 2024; Jiang et al., 2025). Some studies have also considered the morphology of individual BC-containing particle and developed advanced models such as the electron-microscope-to-BC-simulation (EMBS) (Wang et al., 2021c; Wang et al., 2021b; Chakrabarty et al., 2006), thereby enhancing the accuracy of modeled BC E_{abs}. Although the improved model proposed in this study demonstrates better fitting performance especially under low PM_1 concentrations conditions (clean periods, Case 1), its accuracy remains highly dependent on the classification of the "transition state." During heavily polluted periods or in highly polluted regions (Case 2 and Case 3), the "transition state" is usually concentrated within a smaller M_R range, whereas under clean periods, it usually appears in a larger M_R range. If a uniform classification of "transition state" is applied, it will inevitably introduce errors in modeled BC E_{abs} (Fig. 4b, 4c and 4c). Moreover, considering only the M_R heterogeneity of BC-containing particle can effectively reproduce the observed BC E_{abs} in polluted environments. However, applying different model input schemes to varying atmospheric conditions would increase the complexity of radiation model. Therefore, a unified model input scheme that incorporates both M_R heterogeneity and morphology is recommended for all atmospheric conditions. This model input scheme allows for a more consistent representation of BC mixing state while focusing solely on how environmental variations influence the classification of the "transition state". In summary, improvements to the model should not only account for the M_R heterogeneity, morphological differences of BC-containing particle but also incorporate the dynamic changes in environmental conditions to more accurately predict the optical

https://doi.org/10.5194/egusphere-2025-2844
Preprint. Discussion started: 30 June 2025

properties of BC-containing particles in different atmospheric environments, thereby reducing errors in assessing the climate effects of BC.

4 Conclusions

In this study, we employed the CPMA-SP2 tandem system to investigate the mass ratio of coating and core (M_R), and morphology of BC-containing particles in Hangzhou, China, and to assess how heterogeneity in M_R and morphology influence their E_{abs} under different atmospheric conditions. By dividing the observation into three representative scenarios (Case 1, Case 2, and Case 3), we observed significant differences in the measured E_{abs}, that were closely associated with the evolution and distribution of M_R and morphology characteristics. The findings indicate that both M_R heterogeneity and morphology play critical roles in modeling E_{abs}. During clean condition (Case 1), the uniform core-shell Mie model significantly overestimated E_{abs}, while during polluted periods (Case 2 and Case 3), model predictions were more consistent with the measured E_{abs}. To address these discrepancies, we developed a morphology-dependent correction scheme for the optical property calculation of BC in the "transition state" by incorporating M_R heterogeneity and morphology information. The improved model input method effectively reconciled the measured E_{abs} across varying pollution conditions, especially in clean environments dominated by externally mixed and partially coated BC-containing particles. Our results further show that environmental factors-such as the chemical composition of PM_1-not only influence the morphology and M_R distribution of BC-containing particles but also shift the threshold M_R range defining the "transition state". These findings underscore the limitations of uniform model input schemes under complex atmospheric conditions and demonstrate the value of a unified modeling framework that incorporates both M_R heterogeneity and particle morphology. Such improvement enables more accurate representation of BC mixing state and light absorption across diverse environmental settings, thereby reducing uncertainties in assessing the radiative forcing of BC-containing particles.

Data availability. The data are available from the link: http://doi.org/10.6084/m9.figshare.29097263.

Author contributions.

Conceptualization: Jing Wei, Zhi-Bin Wang
Data curation: Jing Wei, Yao Song, Xiang-Yu Pei, Fei Zhang, Zheng-Ning Xu, Jin-Mei Ding, Xiao-Yuan Wang, Sheng-Chen Xu, Xu-Dong Tian, Bing-Ye Xu
Formal analysis: Jing Wei
Funding acquisition: Zhi-Bin Wang, Bing-Ye Xu
Investigation: Zhi-Bin Wang
Methodology: Jing Wei, Zhi-Bin Wang
Visualization: Jing Wei, Zhi-Bin Wang
Writing – original draft: Jing Wei

https://doi.org/10.5194/egusphere-2025-2844
Preprint. Discussion started: 30 June 2025

Competing interests. At least one of the (co-)authors is a member of the editorial board of *Atmospheric Chemistry and Physics*.

Financial support. This research was supported by the Joint Fund of Zhejiang Provincial Natural Science Foundation of China (LZJMZ25D050003), the National Key Research and Development Program of China (2022YFC3703505), the National Natural Science Foundation of China (42305098), the China Postdoctoral Science Foundation (2023M733028), the Key Laboratory of Formation and Prevention of Urban Air Pollution Complex, Ministry of Ecology and Environment (2025080166).

References

Bauer, S. E., Ault, A. P., and Prather, K. A.: Evaluation of aerosol mixing state classes in the GISS modelE-MATRIX climate model using single-particle mass spectrometry measurements, Journal of Geophysical Research: Atmospheres, 118, 9834-9844, 10.1002/jgrd.50700, 2013.

Bond, T. C. and Bergstrom, R. W.: Light Absorption by Carbonaceous Particles: An Investigative Review, Aerosol Science and Technology, 40, 27-67, 10.1080/02786820500421521, 2006.

Brooks, J., Liu, D., Allan, J. D., Williams, P. I., Haywood, J., Highwood, E. J., Kompalli, S. K., Babu, S. S., Satheesh, S. K., Turner, A. G., and Coe, H.: Black carbon physical and optical properties across northern India during pre-monsoon and monsoon seasons, Atmospheric Chemistry and Physics, 19, 13079-13096, 10.5194/acp-19-13079-2019., 2019.

Cappa, C. D., Zhang, X., Russell, L. M., Collier, S., Lee, A. K. Y., Chen, C. L., Betha, R., Chen, S., Liu, J., Price, D. J., Sanchez, K. J., McMeeking, G. R., Williams, L. R., Onasch, T. B., Worsnop, D. R., Abbatt, J., and Zhang, Q.: Light Absorption by Ambient Black and Brown Carbon and its Dependence on Black Carbon Coating State for Two California, USA, Cities in Winter and Summer, Journal of Geophysical Research: Atmospheres, 124, 1550-1577, 10.1029/2018JD029501, 2019.

Cappa, C. D., Onasch, T. B., Massoli, P., Worsnop, D. R., Bates, T. S., Cross, E. S., Davidovits, P., Hakala, J., Hayden, K. L., Jobson, B. T., Kolesar, K. R., Lack, D. A., Lerner, B. M., Li, S.-M., Mellon, D., Nuaaman, I., Olfert, J. S., Petäjä, T., Quinn, P. K., Song, C., Subramanian, R., Williams, E. J., and Zaveri, R. A.: Radiative Absorption Enhancements Due to the Mixing State of Atmospheric Black Carbon, Science, 337, 1078-1081, https://doi.org/10.1126/science.1223447, 2012.

Chakrabarty, R. K., Moosmueller, H., Arnott, W. P., Garro, M. A., and Walker, J.: Structural and fractal properties of particles emitted from spark ignition engines, Environmental Science & Technology, 40, 6647-6654, 10.1021/es060537y, 2006.

Chen, G., Liu, C., Wang, J., Yin, Y., and Wang, Y.: Accounting for Black Carbon Mixing State, Nonsphericity, and Heterogeneity Effects in Its Optical Property Parameterization in a Climate Model, Journal of Geophysical Research: Atmospheres, 129, e2024JD041135, 10.1029/2024JD041135, 2024.

Fierce, L., Onasch, T. B., Cappa, C. D., Mazzoleni, C., China, S., Bhandari, J., Davidovits, P., Al Fischer, D., Helgestad, T., Lambe, A. T., Sedlacek, A. J., Smith, G. D., Wolff, L., Brookhaven National Lab, U. N. Y., and Pacific Northwest National Lab, R. W. A.: Radiative absorption enhancements by black carbon controlled by particle-to-particle heterogeneity in composition, Proceedings of the National Academy of Sciences, 117, 5196-5203, 10.1073/pnas.1919723117, 2020.

Gao, R. S., Schwarz, J. P., Kelly, K. K., Fahey, D. W., Watts, L. A., Thompson, T. L., Spackman, J. R., Slowik, J. G., Cross, E. S., Han, J. H., Davidovits, P., Onasch, T. B., and Worsnop, D. R.: A Novel

https://doi.org/10.5194/egusphere-2025-2844
Preprint. Discussion started: 30 June 2025

Method for Estimating Light-Scattering Properties of Soot Aerosols Using a Modified Single-Particle Soot Photometer, Aerosol Science and Technology, 41, 125-135, 10.1080/02786820601118398, 2007.

Huang, X.-F., Peng, Y., Wei, J., Peng, J., Lin, X.-Y., Tang, M.-X., Cheng, Y., Men, Z., Fang, T., Zhang, J., He, L.-Y., Cao, L. M., Liu, C., Zhang, C., Mao, H., Seinfeld, J. H., and Wang, Y.: Microphysical complexity of black carbon particles restricts their warming potential, One Earth, 7, 10.1016/j.oneear.2023.12.004, 2024.

Jiang, F., Zheng, Z., Coe, H., Healy, R. M., Poulain, L., Gros, V., Zhang, H., Li, W., Liu, D., West, M., Topping, D., and Riemer, N.: Integrating Simulations and Observations: A Foundation Model for Estimating the Aerosol Mixing State Index, Environmental Science & Technology Air, 10.1021/acsestair.4c00329, 2025.

Kahnert, M. and Kanngießer, F.: Modelling optical properties of atmospheric black carbon aerosols, Journal of Quantitative Spectroscopy & Radiative Transfer, 244, 106849, 10.1016/j.jqsrt.2020.106849, 2020.

Li, W., Riemer, N., Xu, L., Wang, Y., Adachi, K., Shi, Z., Zhang, D., Zheng, Z., and Laskin, A.: Microphysical properties of atmospheric soot and organic particles: measurements, modeling, and impacts, npj Climate and Atmospheric Science, 7, 65, 10.1038/s41612-024-00610-8, 2024.

Liu, D., Taylor, J. W., Young, D. E., Flynn, M. J., Coe, H., and Allan, J. D.: The effect of complex black carbon microphysics on the determination of the optical properties of brown carbon: BC morphology on BrC optical properties, Geophysical Research Letters, 42, 613-619, 10.1002/2014GL062443, 2015.

Liu, D., Allan, J. D., Young, D. E., Coe, H., Beddows, D., Fleming, Z. L., Flynn, M. J., Gallagher, M. W., Harrison, R. M., Lee, J., Prevot, A. S. H., Taylor, J. W., Yin, J., Williams, P. I., and Zotter, P.: Size distribution, mixing state and source apportionment of black carbon aerosol in London during wintertime, Atmospheric Chemistry and Physics, 14, 10061-10084, 10.5194/acp-14-10061-2014, 2014.

Liu, D., Whitehead, J., Alfarra, M. R., Reyes-Villegas, E., Spracklen, D. V., Reddington, C. L., Kong, S., Williams, P. I., Ting, Y.-C., Haslett, S., Taylor, J. W., Flynn, M. J., Morgan, W. T., McFiggans, G., Coe, H., and Allan, J. D.: Black-carbon absorption enhancement in the atmosphere determined by particle mixing state, Nature Geoscience, 10, 184-188, 10.1038/ngeo2901, 2017.

Liu, H., Pan, X., Liu, D., Liu, X., Chen, X., Tian, Y., Sun, Y., Fu, P., and Wang, Z.: Mixing characteristics of refractory black carbon aerosols at an urban site in Beijing, Atmospheric Chemistry and Physics, 20, 5771-5785, 10.5194/acp-20-5771-2020, 2020.

Moteki, N. and Kondo, Y.: Effects of Mixing State on Black Carbon Measurements by Laser-Induced Incandescence, Aerosol Science and Technology, 41, 398-417, 10.1080/02786820701199728, 2007.

Peng, J., Hu, M., Guo, S., Du, Z., Zheng, J., Shang, D., Zamora, M. L., Zeng, L., Shao, M., Wu, Y.-S., Zheng, J., Wang, Y., Glen, C. R., Collins, D. R., Molina, M. J., and Zhang, R.: Markedly enhanced absorption and direct radiative forcing of black carbon under polluted urban environments, Proceedings of the National Academy of Sciences, 113, 4266-4271, 10.1073/pnas.1602310113, 2016.

Romshoo, B., Müller, T., Ahlawat, A., Wiedensohler, A., Haneef, M. V., Imran, M., Warsi, A. B., Mandariya, A. K., Habib, G., and Pöhlker, M. L.: Significant contribution of fractal morphology to aerosol light absorption in polluted environments dominated by black carbon (BC), npj Climate and Atmospheric Science, 7, 87, 10.1038/s41612-024-00634-0, 2024.

https://doi.org/10.5194/egusphere-2025-2844
Preprint. Discussion started: 30 June 2025

Schloesser, H.: Use of a Multi-Wavelength Integrating Nephelometer to Determine Source Influences on Particle Concentration Measurements. Atmospheric optics: aerosols, visibility and the radiatiov balance 2016, vol. 1: Atmospheric optics conference, 27-30 September 2016, Jackson Hole, Wyoming, USA., 2016.

Seinfeld, J.: Atmospheric science - Black carbon and brown clouds, Nature Geoscience, 1, 15-16, 10.1038/ngeo.2007.62, 2008.

Stier, P., Feichter, J., Kinne, S., Kloster, S., Vignati, E., Wilson, J., Ganzeveld, L., Tegen, I., Werner, M., Balkanski, Y., Schulz, M., Boucher, O., Minikin, A., and Petzold, A.: The aerosol-climate model ECHAM5-HAM, Atmospheric Chemistry and Physics, 5, 1125-1156, 10.5194/acp-5-1125-2005, 2005.

Szopa, S., Naik, V., Adhikary, B., Artaxo, P., Berntsen, T., Collins, W. D., Fuzzi, S., Gallardo, L., Kiendler-Scharr, A., Klimont, Z., Liao, H., Unger, N., and Zanis, P.: Short-Lived Climate Forcers. In Climate Change 2021: The Physical Science Basis. Contribution of Working Group I to the Sixth Assessment Report of the Intergovernmental Panel on Climate Change (eds Masson-Delmotte, V. et al.), IPCC, 2021.

Wang, J., Wang, J., Cai, R., Liu, C., Jiang, J., Nie, W., Wang, J., Moteki, N., Zaveri, R. A., Huang, X., Ma, N., Chen, G., Wang, Z., Jin, Y., Cai, J., Zhang, Y., Chi, X., Holanda, B. A., Xing, J., Liu, T., Qi, X., Wang, Q., Pöhlker, C., Su, H., Cheng, Y., Wang, S., Hao, J., Andreae, M. O., and Ding, A.: Unified theoretical framework for black carbon mixing state allows greater accuracy of climate effect estimation, Nature Communications, 14, 2703, 10.1038/s41467-023-38330-x, 2023.

Wang, T. T., Zhao, G., Tan, T. Y., Yu, Y., Tang, R. Z., Dong, H. B., Chen, S. Y., Li, X., Lu, K. D., Zeng, L. M., Gao, Y. Q., Wang, H. L., Lou, S. R., Liu, D. T., Hu, M., Zhao, C. S., and Guo, S.: Effects of biomass burning and photochemical oxidation on the black carbon mixing state and light absorption in summer season, Atmospheric Environment, 248, 10.1016/j.atmosenv.2021.118230, 2021a.

Wang, Y., Pang, Y., Huang, J., Bi, L., Che, H., Zhang, X., and Li, W.: Constructing Shapes and Mixing Structures of Black Carbon Particles With Applications to Optical Calculations, Journal of Geophysical Research: Atmospheres, 126, 10.1029/2021jd034620, 2021b.

Wang, Y., Li, W., Huang, J., Liu, L., Pang, Y., He, C., Liu, F., Liu, D., Bi, L., Zhang, X., and Shi, Z.: Nonlinear Enhancement of Radiative Absorption by Black Carbon in Response to Particle Mixing Structure, Geophysical Research Letters, 48, 10.1029/2021gl096437, 2021c.

Weber, P., Petzold, A., Bischof, O. F., Fischer, B., Berg, M., Freedman, A., Onasch, T. B., and Bundke, U.: Relative errors in derived multi-wavelength intensive aerosol optical properties using cavity attenuated phase shift single-scattering albedo monitors, a nephelometer, and tricolour absorption photometer measurements, Atmospheric Measurement Techniques, 15, 3279-3296, 10.5194/amt-15-3279-2022, 2022.

Wu, Y., Cheng, T., and Zheng, L.: Light absorption of black carbon aerosols strongly influenced by particle morphology distribution, Environmental Research Letters, 15, 94051, 10.1088/1748-9326/aba2ff, 2020.

Zeng, L., Tan, T., Zhao, G., Du, Z., Hu, S., Shang, D., and Hu, M.: Overestimation of black carbon light absorption due to mixing state heterogeneity, npj Climate and Atmospheric Science, 7, 2, 10.1038/s41612-023-00535-8, 2024.

Zhai, J., Yang, X., Li, L., Bai, B., Liu, P., Huang, Y., Fu, T.-M., Zhu, L., Zeng, Z., Tao, S., Lu, X., Ye, X., Wang, X., Wang, L., and Chen, J.: Absorption Enhancement of Black Carbon Aerosols Constrained by Mixing-State Heterogeneity, Environmental Science & Technology, 56, 1586-1593,

https://doi.org/10.5194/egusphere-2025-2844
Preprint. Discussion started: 30 June 2025

10.1021/acs.est.1c06180, 2022.

Zhang, J., Wang, Y., Teng, X., Liu, L., Xu, Y., Ren, L., Shi, Z., Zhang, Y., Jiang, J., Liu, D., Hu, M., Shao, L., Chen, J., Martin, S. T., Zhang, X., and Li, W.: Liquid-liquid phase separation reduces radiative absorption by aged black carbon aerosols, Communications Earth & Environment, 3, 128, 10.1038/s43247-022-00462-1, 2022.

Zhang, Y., Zhang, Q., Cheng, Y., Su, H., Li, H., Li, M., Zhang, X., Ding, A., and He, K.: Amplification of light absorption of black carbon associated with air pollution, Atmospheric Chemistry and Physics, 18, 9879-9896, 10.5194/acp-18-9879-2018, 2018.

Zhang, Y., Zhang, Q., Cheng, Y., Su, H., Kecorius, S., Wang, Z., Wu, Z., Hu, M., Zhu, T., Wiedensohler, A., and He, K.: Measuring the morphology and density of internally mixed black carbon with SP2 and VTDMA: new insight into the absorption enhancement of black carbon in the atmosphere, Atmospheric Measurement Techniques, 9, 1833-1843, 10.5194/amt-9-1833-2016, 2016.

Zhang, Y. X., Zhang, Q., Yao, Z. L., and Li, H. Y.: Particle Size and Mixing State of Freshly Emitted Black Carbon from Different Combustion Sources in China, Environmental Science & Technology, 54, 7766-7774, 10.1021/acs.est.9b07373, 2020.

Zhang, Z., Wang, J., Wang, J., Riemer, N., Liu, C., Jin, Y., Tian, Z., Cai, J., Cheng, Y., Chen, G., Wang, B., Wang, S., and Ding, A.: Steady-state mixing state of black carbon aerosols from a particle-resolved model, Atmospheric Chemistry and Physics, 25, 1869-1881, 10.5194/acp-25-1869-2025, 2025.

Zhao, G., Shen, C., and Zhao, C.: Technical note: Mismeasurement of the core-shell structure of black carbon-containing ambient aerosols by SP2 measurements, Atmospheric Environment, 243, 117885, 10.1016/j.atmosenv.2020.117885, 2020.